Structure of Gremlin-1 and analysis of its interaction with BMP-2

Miglė Kišonaitė*, Xuelu Wang* and Marko Hyvönen*[1]

*Department of Biochemistry, University of Cambridge, 80 Tennis Court Road, Cambridge CB2 1GA, U.K.

Bone morphogenetic protein 2 (BMP-2) is a member of the transforming growth factor-β (TGF-β) signalling family and has a very broad biological role in development. Its signalling is regulated by many effectors: transmembrane proteins, membrane-attached proteins and soluble secreted antagonists such as Gremlin-1. Very little is known about the molecular mechanism by which Gremlin-1 and other DAN (differential screening-selected gene aberrative in neuroblastoma) family proteins inhibit BMP signalling. We analysed the interaction of Gremlin-1 with BMP-2 using a range of biophysical techniques, and used mutagenesis to map the binding site on BMP-2. We have also determined the crystal structure of Gremlin-1, revealing a similar conserved dimeric structure to that seen in other DAN family inhibitors. Measurements using biolayer interferometry (BLI) indicate that Gremlin-1 and BMP-2 can form larger complexes, beyond the expected 1:1 stoichiometry of dimers, forming oligomers that assemble in alternating fashion. These results suggest that inhibition of BMP-2 by Gremlin-1 occurs by a mechanism that is distinct from other known inhibitors such as Noggin and Chordin and we propose a novel model of BMP-2–Gremlin-1 interaction yet not seen among any BMP antagonists, and cannot rule out that several different oligomeric states could be found, depending on the concentration of the two proteins.

Key words: bone morphogenetic protein (BMP), differential screening-aberrative in neuroblastoma (DAN), extracellular antagonism, Gremlin, structural biology, transforming growth factor-β (TGF-β), X-ray crystallography.

INTRODUCTION

Gremlin-1 is an extracellular antagonist of the bone morphogenetic proteins (BMPs) and functions by directly neutralizing its ligands and inhibiting BMP signalling [1–4]. BMPs, together with their antagonists, are responsible for regulating many important processes during early embryonic development [5–11], and have broad and complex biological roles [3,12–14]. Signal propagation by BMPs is initiated when a dimer of the mature BMP binds to two types of serine/threonine kinase receptors, a specific high-affinity type I receptor and a lower-affinity type II receptor. With only seven type I and five type II receptors for over 30 transforming growth factor-β (TGF-β)-like ligands in humans, several ligands can interact with any particular receptor but at the same time one ligand can interact with several type I and type II receptors [15–17]. This results in high complexity of signalling and also raises the question as to how BMPs can exert so many cellular functions and highlights the need for another level of signalling modulators that could attenuate the levels of active BMP [18,19]. In the case of BMPs, one of the key mechanisms of signal regulation is via the interaction with secreted antagonists such as Noggin, Chordin [3,20] and Gremlin-1, which can specifically bind to BMPs and prevent their interaction with receptors [21].

Gremlin-1 belongs to the DAN family of secreted BMP antagonists. This family, named after the prototypical member Dan (differential screening-selected gene aberrative in neuroblastoma), also contains proteins Cerberus, Gremlin-1, Gremlin-2 (also called protein related to Dan and Cerberus, PRDC), Coco, Sclerostin and uterine sensitization-associated gene-1 (USAG-1) [1–4]. BMP antagonists have many roles in development and are also implicated in many disorders [6]. In lungs Gremlin-1 overexpression inhibits BMP-7, resulting in myofibroblast apoptosis and fibrotic response, whereas in hepatic stellate cells an increase in Gremlin-1 expression contributes to liver failure [4,22–24]. Gremlin-1 is also expressed at the base of intestinal crypts, helping to maintain the stem cell pool by countering the BMP activity that arises from the mesenchymal cells [25]. Overexpression of Gremlin-1 has also been shown in stromal cells in tumours, where it helps to create a favourable niche for the cancer cells to grow in [26,27].

The first DAN family protein to have its 3D structure determined was Sclerostin [28,29]. The solution NMR structure of Sclerostin revealed a monomeric protein containing a cystine knot core and an elongated shape comprising two β-stranded fingers on one side of the central cystine knot and three flexible loops on the opposite side. More recently, the crystal structures of Gremlin-2 and Dan have also been determined [30,31]. The structure of Gremlin-2 revealed a non-covalent dimer that forms through extensive hydrogen bonding between the β-sheets of its two protomers [31]. Dan shares a similar architecture, with an identical mode of non-covalent dimerization [32]. To date, no structures of DAN family proteins in complex with BMPs have been published and it remains unclear how they inhibit BMP signalling at the molecular level. Do these antagonists act by blocking one or both receptor-binding sites, as has been shown to be the case for Noggin and CV-2 (Crossveinless-2) [20,33], or do they reveal a different mode of inhibition altogether? Dan-like proteins are structurally distinct from other BMP inhibitors,

Abbreviations: AP, alkaline phosphatase; ASU, asymmetric unit; AUC, analytical ultracentrifugation; BLI, biolayer interferometry; BMP, bone morphogenetic protein; BMPR, BMP receptor; CV-2, crossveinless-2; DAM, dummy atom model; DAN, differential screening-selected gene aberrative in neuroblastoma; DLS, dynamic light scattering; DMEM, Dulbecco's modified Eagle's medium; MALS, multi-angle light scattering; PPS, 3-(1-pyridino)-1-propanesulfonate; PRDC, protein related to Dan and Cerberus; RGM, repulsive guidance molecule; RPC, reverse-phase chromatography; SAXS, small-angle X-ray scattering; TCEP, tris-(2-carboxyethyl)phosphine; TFA, trifluoroacetic acid; TGF-β, transforming growth factor-β; USAG-1, uterine sensitization-associated gene-1; VWC1, von Willebrand factor type C domain 1.

[1] To whom correspondence should be addressed (email mh256@cam.ac.uk).

and the structures of Dan, Gremlin-2 and Sclerostin have so far provided few clues about the molecular mechanism and specificity of inhibition.

To broaden our understanding of DAN family BMP antagonism, we have studied the mechanism of BMP inhibition by Gremlin-1 and determined its crystal structure. Analytical ultracentrifugation (AUC), dynamic light scattering (DLS) and analyses of the interaction between BMP-2 mutants and Gremlin-1 have been used to delineate the molecular details of the binding mechanism. Based on our findings, we propose a model of BMP-2–Gremlin-1 interaction through formation of larger oligomeric complexes.

EXPERIMENTAL

Protein expression, refolding and purification

Constructs of Gremlin-1 (UniProt #O60565) were amplified by PCR using human Gremlin-1 cDNA as template (a gift from Dr Katri Koli, University of Helsinki, Helsinki, Finland) with primers listed in Supplementary Table S1. The fragments encoding full-length construct (fl-Gremlin-1, residues 25–184, lacking only its signal sequence) and a shorter one (ΔN-Gremlin-1, residues 72–184) were cloned as *BspHI*/*Hind*III fragments into pHAT4 and pBAT4 vectors and confirmed by sequencing. The pHAT4 constructs contain an N-terminal hexahistidine tag with TEV protease cleavage site, whereas the pBAT4 constructs are untagged. A synthetic *Escherichia coli* codon-optimized gene encoding mature BMP-2 was cloned into pBAT4 vector [34]. PCR-based site-directed mutagenesis was used to introduce desired BMP-2 mutations. All proteins were expressed in *E. coli* strain BL21(DE3), which in the case of Gremlin-1 expression was also carrying plasmid pUBS520 to compensate for codon usage differences [35]. Bacteria were grown in 2 YT medium [1.6 % (w/v) tryptone, 1 % (w/v) yeast extract and 0.5 % NaCl] at 37 °C until the D_{600} reached 0.8–1.0, after which expression was induced by addition of 400 uM IPTG and continued for 3 h. Pelleted cells were resuspended in water and stored at −20 °C.

All constructs of Gremlin-1, as well as BMP-2 and mutant variants, were expressed insolubly and subsequently refolded to active form. Gremlin-1 inclusion bodies were solubilized in 6 M guanidinium chloride, 25 mM TCEP [tris-(2-carboxyethyl)phosphine], 50 mM Tris/HCl, pH 8.0, and 0.5 mM EDTA and refolded by rapid dilution into refolding buffer containing 1 M PPS [3-(1-pyridino)-1-propanesulfonate], 50 mM Tris/HCl, pH 8.0, 50 mM ethylenediamine, 2 mM EDTA, 2 mM cysteine and 0.2 mM cystine and left for 7 days at 4 °C. Gremlin-1 was purified by ion-exchange chromatography using a HiTrap SP HP 5 ml column (GE Healthcare) equilibrated with 20 mM Hepes, pH 7.0. Filtered refolding solution was loaded directly on to the column and washed with the equilibration buffer, and bound proteins were eluted using a linear gradient to 1 M NaCl. Pooled fractions from the ion exchange were acidified and purified further by reverse-phase chromatography (RPC) using ACE 5 C8-300 column (Hichrom) that was equilibrated with 10 % acetonitrile, 0.1 % trifluoroacetic acid (TFA). Bound protein was eluted using a linear 20–40 % gradient in 10 column volumes, with 90 % acetonitrile and 0.1 % TFA.

For the refolding of BMP-2 and its mutants, the inclusion bodies were solubilized using 10 mM TCEP, 6 M guanidinium chloride, 0.5 mM EDTA and 50 mM Tris/HCl, pH 8.0 and refolded in 1 M PPS, 100 mM Tris/HCl, pH 8.0, 100 mM ethylendiamine, 300 mM NaCl, 0.5 mM EDTA, 2 mM cysteine and 0.2 mM cystine. Solubilized inclusion bodies were added to the refolding buffer in small aliquots with 6 days in between and kept at 4 °C for up to 2 weeks to allow disulfide exchange. BMP-2 variants were purified by RPC using a 10 ml Source RPC 15 (GE Healthcare) column by loading refolded material directly on to the column and eluting bound proteins using a linear gradient of 10–45 % acetonitrile (with 0.1 % TFA) in 13 column volumes. All protein concentrations were determined by absorbance at 280 nm using calculated molecular absorption coefficients of 11 960 $mol^{-1} \cdot cm^{-1}$ for both Gremlin-1 proteins and 18 825 $mol^{-1} \cdot cm^{-1}$ for BMP-2s. BMP-2 and its mutants were lyophilized after purification by RPC and resuspended to a protein concentration of 0.15 mg/ml in MilliQ water. CD spectrum at 189–250 nm was measured for each of the proteins three times. Each scan was baseline corrected and the three measurements were averaged and smoothened to produce the final CD spectra. Secondary structure content was estimated using K2D3 server at http://cbdm-01.zdv.uni-mainz.de/~andrade/k2d3/.

Multi-angle light scattering (MALS) experiments were carried out with a DAWN HELEOS 8 detector with a wavelength of 664 nm and Optilab T-rEX refractometer (Wyatt Technology). MALS analysis was performed using a Superdex 200 Increase 10/300 (GE Healthcare) column equilibrated with PBS (137 mM NaCl, 3 mM KCl, 8 mM Na_2HPO_4 and 15 mM KH_2PO_4) containing an additional 0.4 M NaCl, 0.5 M L-arginine and 5 % glycerol, pH 8.0. All samples were loaded on to the column at a concentration of 1 mg/ml. Data were analysed with ASTRA software (Wyatt Technology) and molecular mass was calculated using a Debye fit model.

Interaction and bioactivity assays

Biolayer interferometry (BLI) using an Octet RED96 (PallGelman/ForteBio) instrument was used for the analysis of BMP-2–Gremlin-1 interactions. All experiments were performed using anti-pentahistidine antibody biosensors (PallGelman/ForteBio), which were regenerated at most eight times with 10 mM glycine pH 1.7. All samples were prepared in kinetics buffer (1 PBS, pH 7.4, 0.01 % BSA, 0.002 % Tween 20, 400 mM NaCl and 0.02 % P20). A schematic diagram of the experimental set-up is shown in Supplementary Table S2. Data were processed using ForteBio Data Analysis 7.1 software and fitted using Origin Pro 9.0 package.

BMP-2 bioactivity assays were completed using C2C12 mouse myoblasts which can be induced to secrete alkaline phosphatase (AP) by BMP-2 [36]. C2C12 cells at passages 5–10 were subcultured in DMEM (Dulbecco's modified Eagle's medium) containing 10 % FBS at 37 °C in a humidified atmosphere of 5 % CO_2 in air. For AP assay, cells were diluted to 5000 cells/ml and divided into aliquots in 96-well plates. Plates were treated with BMP-2 and Gremlin-1 the following day. Serial dilutions of proteins were performed in sterile DMEM. After 48 h, the cells were washed with PBS and lysed by addition of 0.56 M 2-amino-2-methyl-propan-1-ol and 0.1 % SDS, pH 10.0. AP activity was measured by adding the substrate pNPP (*p*-nitrophenyl phosphate), which develops a soluble yellow reaction product, and absorbance was read at 405 nm using a BMG PHERAstar FS plate reader. All C2C12 experiments were repeated six times. Data were analysed using Origin Pro 9.0 software.

Structural studies

His-tagged ΔN-Gremlin-1 was used for crystallization at 8 mg/ml concentration in 20 mM Hepes, pH 8.0. Crystals formed in 2.1 M NaCl, 0.1 M sodium acetate, pH 4.5, and 0.3 M $LiSO_4$. For data collection, the crystals were cryo-cooled in liquid N_2

in the crystallization solution containing 30 % ethylene glycol as a cryoprotectant. Data were collected at beamline I04 at the Diamond Light Source. Collected data were integrated and analysed using autoPROC software package [37]. The phases were found by molecular replacement with the structure of Gremlin-2 (PDB code: 4JPH) using Amore package in the CCP4 suite [38]. The model was manually corrected using Coot 0.8.1 [39] and refined with Refmac5 [38]. The co-ordinates and structure factors have been deposited in the PDB under accession number 5AEJ.

Samples for small-angle X-ray scattering (SAXS) were measured at 1 mg/ml concentrations in PBS with 0.4 M NaCl, 0.5 M L-arginine and 5 % glycerol using Superdex 200 3.2/300 Increase size-exclusion column (GE Healthcare) with inline data collection chromatography run. Data were collected at beamline I22 at the Diamond Light Source. Data processing and analysis was performed using Scatter and ATSAS suite software [40].

Analytical ultracentrifugation

AUC was performed using a Beckman Optima XL-I instrument using both UV and interference optics. ΔN-Gremlin-1, BMP-2 and mixture of both proteins were dialysed overnight against reference buffer (100 mM sodium acetate, pH 5.0) before centrifugation and used at concentrations of 1 mg/ml. Data were analysed using Sedfit [41].

RESULTS

Gremlin-1 interaction with BMP-2 and functional activity assays

DAN protein family members are typically composed of 180–270 amino acid residues (excluding signal peptide). Overall sequence identity between any two DAN proteins tends to be relatively low, at 10–30 %, increasing by some 10 % if we consider the C-terminal cystine knot domain only (alignment of human DAN family proteins are shown in Supplementary Figure S1). Two pairs of Dan family members share higher than average pairwise sequence identity in their cysteine-rich domains: Gremlin-1 and -2 (65 %) and Sclerostin and USAG-1 (45 %). The N-terminal parts of the proteins, outside the cystine knot domains, differ greatly both in sequence and in length. It is not clear what the role of the N-terminus is, but it is possibly important in determining binding specificity or localization, or is maybe involved in mediating interactions with other proteins [2]. The well-characterized BMP-2 inhibitor Noggin mediates its interaction largely with its N-terminal segment that is not part of the structured cystine knot domain, raising the possibility that DAN proteins function in a similar manner [20].

We have created two constructs of Gremlin-1: a full-length construct (fl-Gremlin-1), comprising residues 25–184 (lacking only the signal peptide), and a shorter one, ΔN-Gremlin-1, comprising residues 72–184, lacking the entire variable N-terminal sequence. This allowed us to investigate the possible role of the N-terminal part of Gremlin-1 in mediating the interaction with BMP-2 and its effect on the inhibition of BMP-2 signalling in mouse myoblasts.

The SDS-PAGE gel in Figure 1(A) shows the purity of all constructs of Gremlin-1 after the final RPC step, with the arrowheads indicating positions of the monomeric Gremlin-1 proteins. On a non-reducing SDS-PAGE gel, Gremlin-1 runs as a characteristic tailed band and some higher oligomeric species are visible, whereas a reducing gel shows one sharp main band with a small proportion of low-molecular-mass contaminants.

First, Gremlin-1 interaction with BMP-2 was analysed using BLI. We immobilized His-tagged fl-Gremlin-1 or ΔN-Gremlin-1 on the biosensors using anti-pentahistidine antibody and measured their interaction with BMP-2 in solution (Figure 1B and Supplementary Figure S2). Measured binding affinities for both constructs with BMP-2 are in close agreement, with K_d values of 5.6 nM and 5.2 nM for fl-Gremlin-1 and ΔN-Gremlin-1 respectively, when data were fitted using a steady-state equilibrium model, and 9.0 nM and 16.7 nM when estimated from kinetic data. The dissociation constant of the BMP-2–Gremlin-1 complex has been previously reported as 32 nM using surface plasmon resonance, which is in good agreement with our values [42].

We then analysed the ability of both full-length and truncated Gremlin-1 to inhibit BMP-2 signalling in C2C12 mouse myoblast cells. BMP-2 induces the differentiation of C2C12 cells into osteoblasts, with an associated increase in secretion of AP which can be readily analysed using a colorimetric enzyme assay [36]. To determine the half maximal effective concentration (EC_{50}) and select an optimal dose of BMP-2 for studying the inhibitory effect of Gremlin-1, C2C12 cells were first treated with BMP-2 alone. We measured an EC_{50} value of 52 nM using this assay, comparable to published values for recombinant BMP-2 [43,44]. In order to measure the inhibitory effect of Gremlin-1, C2C12 cells were treated with a 150 nM concentration of BMP-2 (corresponding to over 90 % activation of the cells) and various concentrations of fl-Gremlin-1 or ΔN-Gremlin-1. Both forms of Gremlin-1 were shown to be active and were able to inhibit BMP-2-induced myoblast differentiation with half maximal inhibitory concentrations (IC_{50}) of 130 nM for fl-Gremlin-1 and 230 nM for ΔN-Gremlin-1 (Figure 1C). In contrast with the affinity measurements of the direct interaction *in vitro* where both proteins were equally potent in binding to BMP-2, the full-length protein had approximately 2-fold higher IC_{50} in this cellular assay. This modest, but reproducible, difference in inhibition suggests that the N-terminal 'clip' region could play a role in the bioactivity of Gremlin-1, possibly by localizing the protein in the extracellular environment and thus facilitating binding to its ligand. The longer construct has a net charge increase in $+4$ compared with the shorter construct and almost a unit higher calculated isoelectric point (9.96 compared with 9.17), possibly contributing to increased affinity towards heparan sulfates, to which both Gremlin-1 and BMP-2 are known to bind [45,46].

Crystal structure of ΔN-Gremlin-1

Given that the N-terminal sequence of Gremlin-1 does not appear to be important for direct interaction with BMP-2, we focused our structure determination efforts on the ΔN-Gremlin-1 construct. This protein crystallized readily and we have determined its structure at 1.9 Å (1 Å = 0.1 nm) resolution (Table 1). The structure was solved by molecular replacement using the structure of Gremlin-2/PRDC as the search model (PDB code: 4JPH) [31] yielding clearly interpretable electron density for all of ΔN-Gremlin-1 and refined to a final model with good final stereochemistry and refinement statistics (Table 1 and Supplementary Figure S3A).

As has been seen with Gremlin-2, Gremlin-1 is a non-covalently linked dimer with overall dimensions of 100 Å × 37 Å × 30 Å (Figure 2A). The overall shape of the Gremlin-1 dimer resembles a bent rod and exposes large convex and concave surfaces (Figures 2B and 2C). The protomer is composed of intertwined antiparallel β-strands with a typical cystine knot core consisting of six cysteine residues. The structure can be described

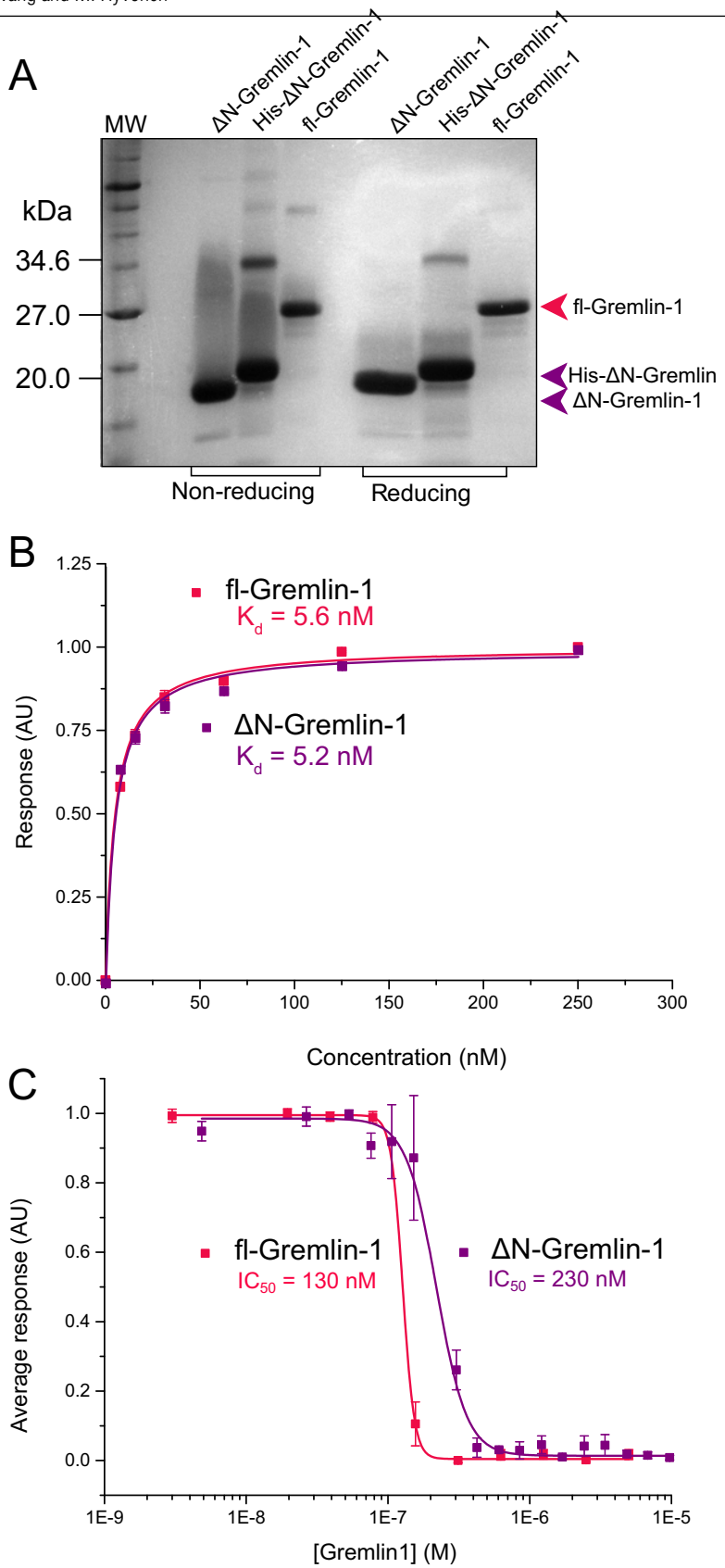

Figure 1 Preparation and functional analysis of Gremlin-1 constructs

(**A**) SDS-PAGE analysis of all Gremlin-1 constructs after final purification: untagged ΔN-Gremlin-1, His-tagged ΔN-Gremlin-1 (lanes 2) and His-tagged fl-Gremlin-1. All samples were analysed under reducing and non-reducing conditions, as indicated. MW, molecular mass (indicated in kDa). (**B**) Gremlin-1 interaction with BMP-2. Equilibrium state binding from BLI for ΔN-Gremlin-1 (purple squares) and fl-Gremlin-1 (pink squares) with BMP-2 data fitted to a steady-state equilibrium model shown as unbroken lines. (**C**) Gremlin-1 inhibition of BMP-2 in C2C12 cells. BMP-2-induced AP activity in C2C12 cells treated with BMP-2–ΔN-Gremlin-1 (purple squares) and BMP-2–Gremlin-1 (pink squares), with the fit to the IC_{50} model shown as unbroken lines. AU, arbitrary units. E = ×10 to the power indicated.

Table 1 X-ray diffraction data and refinement statistics for ΔN-Gremlin-1

Co-ordinates and structure factors have been deposited in the PDB under accession number 5AEJ.

Data collection and processing	
Resolution/highest resolution shell (Å)	41.6–1.9/2.1–1.9
R_{merge}	0.049/0.564
R_{meas}	0.058/0.589
Total number of observations	160 820/23 357
Number of unique reflections	47 349/6881
Mean $I/\delta I$	15.2/2.4
Completeness (%)	99.6/99.3
Multiplicity	3.4/3.4
CC(1/2)	0.999/0.896
Space group	*C2*
Unit cell dimensions:	
a, *b*, *c* (Å)	86.8, 106.1,78.5
α, β, γ (°)	90.0, 121.2, 90.0
Wavelength (Å)	0.97942
Refinement	
Resolution/highest resolution shell (Å)	67.14–1.90/1.95–1.90
Number of reflections	45 041/2779
R_{work}	0.179/0.328
R_{free}	0.208/0.341
Number of non-hydrogen atoms, protein/solvent	3733/201
Average *B*-factor (Å^2)	42.7
RMSD bond length (Å)	0.007
RMSD bond angle (°)	1.04
RMSD planes (°)	0.007
Ramachandran plot: favoured/allowed/outliers	434/12/0

as a composition of two fingers (F1 and F2) and a wrist (W) (Figure 2A). An additional disulfide bond is found in the finger region cross-linking the two fingers. Gremlins, Dan and Sclerostin all share the same arched shape of the protomer (Supplementary Figure S4).

These Gremlin-1 crystals contain two dimers in the asymmetric unit (ASU). The two dimers align very well, and show significant differences only in the finger region, partly driven by crystal contacts (Supplementary Figure S3B). Analysis of the *B*-factors of all chains in the ASU highlights the structural flexibility within the dimers, with the finger loops showing highest *B*-factors, whereas the cores of the dimers are relatively rigid (Supplementary Figure S3C).

The dimerization mode is very similar to other known Dan family members (Gremlin-2 and Dan structures are compared with Gremlin-1 in Supplementary Figures S4A and S4C) with the continuous β-sheets with extensive hydrogen bonding between protomers stabilizing the dimer and producing a 'head-to-tail' structure (Figure 2B). The interactions responsible for strong dimer formation are backbone hydrogen bonds between residues F117 to I127. This interface contains eight hydrogen bonds and constitutes more than half of the interacting surface. Additionally, more than 30 hydrophobic contacts were identified between Gremlin-1 protomers using LigPlot software [47]. In total, a surface area of approximately 1900 Å^2 per protomer is buried upon dimerization, similar to that of Gremlin-2 (~1800 Å^2) [31] (Figure 2C).

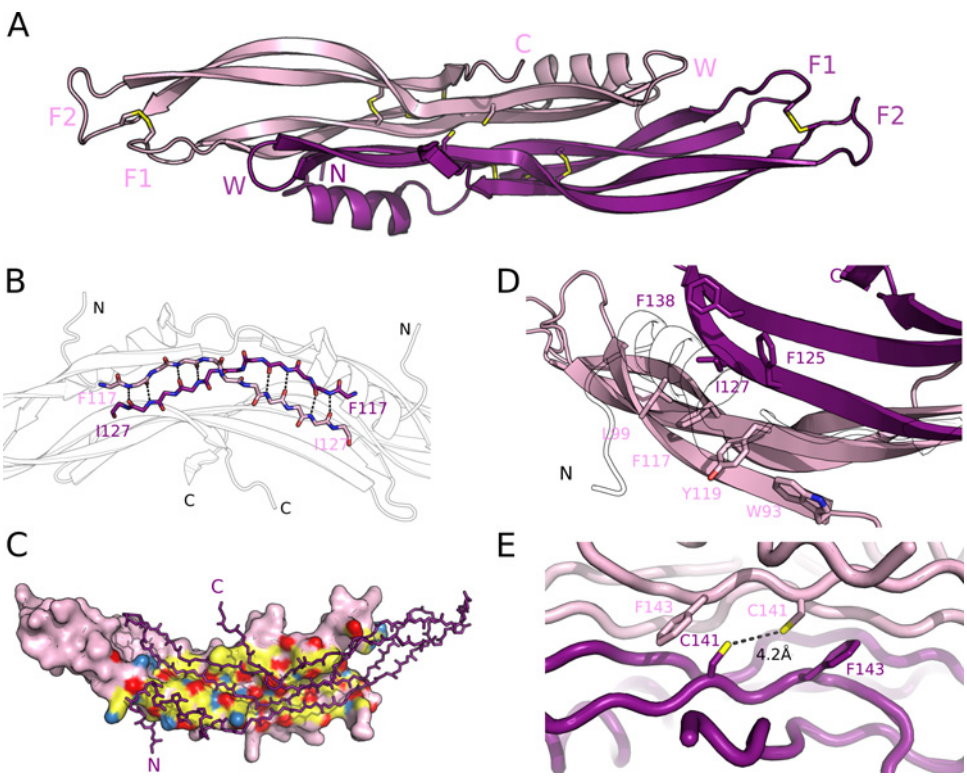

Figure 2 Crystal structure of ΔN-Gremlin-1

(**A**) Cartoon of ΔN-Gremlin-1 dimer with different chains coloured darker and lighter purple, and labelled to indicate parts and motifs discussed in the text. F1 and F2 indicate the fingers, W marks the wrist region and N- and C-termini are labelled N and C, respectively. (**B**) Close-up view of the β-sheet at the dimerization interface. Only the main chain is shown and hydrogen bonds are represented as black dashed lines. (**C**) Dimer of ΔN-Gremlin-1, with one of the two protomers shown with its molecular surface on to which the interaction surface between the protomers is coloured (red for oxygen atoms, blue for nitrogen atoms and yellow for carbons). (**D**) Close-up view of the interfacial α-helix (in transparent outline) with side chains of hydrophobic residues interacting with the helix from both protomers shown as sticks. (**E**) Detailed view of C141 and F143 residues at the dimerization interface.

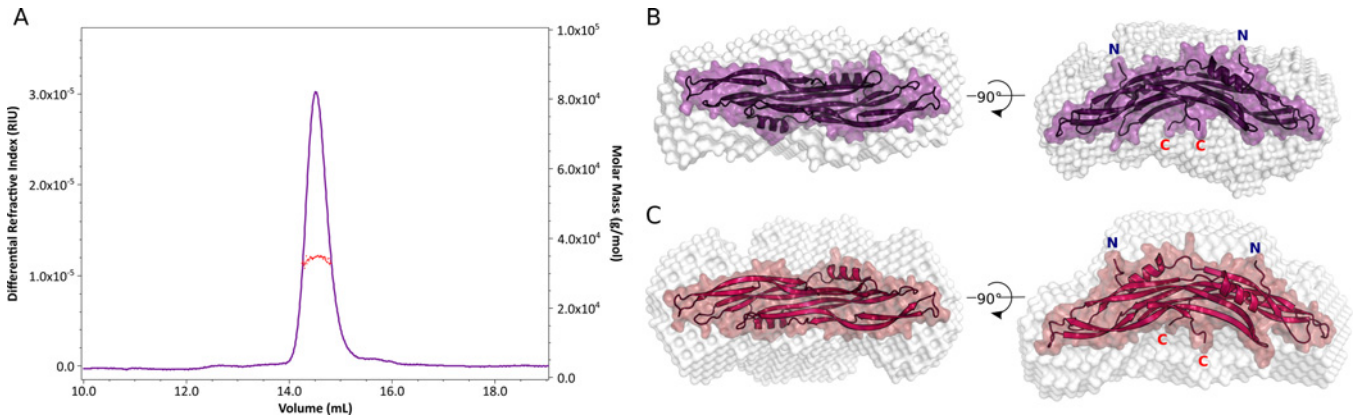

Figure 3 Analysis of oligomeric state of ΔN-Gremlin-1 in solution

(**A**) MALS analysis of ΔN-Gremlin-1 dimer. Light scattering trace is shown as an unbroken line, whereas molecular mass distribution across the peak is shown by red dots. (**B** and **C**) ΔN-Gremlin-1 crystal structure shown as a ribbon and coloured surface with (**B**) ΔN-Gremlin-1 envelope and (**C**) fl-Gremlin-1 envelope shown in white.

In the N-terminus, an α-helix links the interfaces of the protomers. The α-helix plays important role in the interacting surface as well and has intimate contacts with hydrophobic residues of both chains over the shared β-sheet (Figure 2D). The interacting interface is formed by residues F125, I127 and F138 from one protomer and W93, L99 and F117 from the other, with Y88 from the α-helix hydrogen bonding with Q97 of the other protomer. These residues place the helix on top of the convex surface and provide additional interactions between the protomers. In Gremlin-2, this α-helix has high temperature factors and we propose that it does not contribute to the dimer formation. The *B*-factors in Gremlin-1 α-helices are similar to the rest of the structure (Supplementary Figure S3C), suggesting that it is less mobile than in Gremlin-2 and thus likely to contribute to the stabilization of the dimeric structure.

One non-disulfide bonded cysteine (C141) is found close to the dimer interface. In TGF-β family growth factors a similarly positioned cysteine forms a disulfide bridge with another protomer and is responsible for covalent dimerization. In the structure of Gremlin-1, however, C141 does not form a interchain disulfide bridge, despite the close proximity (4.2 Å) of the two thiol groups (Figure 2E and Supplementary Figure S3A). The side chains of F143 flank the cysteines from the each protomer and appear to prevent the formation of a disulfide bridge, as is suggested for Gremlin-2 [31]. Dan protein has an additional cysteine which forms an intra-chain disulfide bond with cysteine equivalent to C141 in Gremlin-1 [30]. It is intriguing that such conserved cysteines are found in close proximity and exposed to solvent. One can speculate that these free cysteines could form disulfides, either within the Gremlin-1 dimer or with another molecule, as part of Gremlins' function in the extracellular matrix.

MALS and SAXS analysis of Gremlin-1

In order to verify that the non-covalent dimeric structure observed in the Gremlin-1 crystals is representative of the solution structure, we used two different solution based methods to confirm this. First, MALS analysis was performed on His-tagged ΔN-Gremlin-1 to determine its molecular mass in solution. The protein is eluted in a single peak from a size-exclusion column and MALS analysis shows that the protein molecular mass of 34.7 kDa, in very good agreement with the predicted mass of 35.0 kDa for dimeric ΔN-Gremlin-1 (Figure 3A).

SAXS analysis was used to validate the overall structure of fl-Gremlin-1 and ΔN-Gremlin-1 in solution. SAXS data were obtained at the Diamond Light Source synchrotron using an inline data collection system during the size-exclusion chromatography run. The linearity of the Guinier plot in the low q region indicates that protein preparations are monodisperse and free of aggregation (Supplementary Figure S5A). Also, the calculated radius of gyration (R_g) values from both reciprocal and real space were highly similar: for ΔN-Gremlin-1 R_g(Rec) = 30.23, R_g(Real) = 30.26, whereas for fl-Gremlin-1 R_g(Rec) = 31.54, R_g(Real) = 31.64. The pair-distance distribution functions $P(r)$ indicate that both long and short constructs of Gremlin-1 have an elongated form with a maximal radius (D_{max}) of 100 Å (Supplementary Figure S5B). The experimental SAXS curves of ΔN-Gremlin-1 and fl-Gremlin-1 as well as simulated curves derived from our crystal structure of the ΔN-Gremlin-1 are in close agreement (Supplementary Figure S5C) with lower chi (χ) score for the dimeric structure compared with isolated monomer both for fl-Gremlin-1 (5.628 for dimer compared with 7.752 for monomer) and for ΔN-Gremlin-1 (1.722 compared with 4.261). This difference is most likely to be due to additional 47 residues in the N-terminus of fl-Gremlin-1, resulting in a poorer fit against the ΔN-Gremlin-1 crystal structure which lacks these residues. Three-dimensional dummy atom models (DAMs) of both constructs were generated from the SAXS curves. Low-resolution envelopes were first generated *ab initio* and aligned with the crystal structure of ΔN-Gremlin-1 (Figures 3B and 3C). From SAXS analysis and overlaid models, it is clear that the overall shape of both constructs of Gremlin-1 in solution are consistent with the dimeric structure seen in the crystal structure. It can also be observed that the envelope of fl-Gremlin-1 occupies more space at the convex face of the protein, suggesting one possible position for the longer N-terminal segment.

Crystallographic analysis, MALS and SAXS all provide consistent results supporting the idea that Gremlin-1 exists as a stable dimer in solution. Although the unique N-terminal portion does not play a key role in the interaction with the growth factor ligand, it also does not significantly alter the overall shape of the domain.

ΔN-Gremlin-1 interaction with BMP-2 mutants

Previously reported mutational analysis of Gremlin-2 showed that mutations in the central convex surface of the protein reduced

Table 2 BMP-2 mutations

Mutated site	Mutant	Mutations
Type I	# 1	49 F → A
	# 2	66 L → R
	# 3	49 F → A, 66 L → R
Type II	# 4	33 V → T, 34 A → S
	# 5	98 V → T, 100 L → N
	# 6	90 L→ Q, 92 L → R
	# 7	33 V → T, 34 A → S, 98 V → T, 100 L → N

its ability to inhibit BMP signalling but still did not reveal the exact mechanism of inhibition [31]. In order to further probe the molecular determinants of the Gremlin-1–BMP-2 interaction, we generated a number of BMP-2 mutants probing both type I and type II receptor-binding sites. Based on the analysis of the BMP-2 quaternary complex with type I and II receptor ectodomain [5], we designed three type I receptor-binding site mutants and four mutants with an altered type II receptor-binding site (Table 2 and Supplementary Figure S6). These seven BMP-2 mutants were expressed and purified for interaction analysis to determine which residues are responsible for Gremlin-1–BMP-2 complex formation. All mutants refolded efficiently and purified as disulfide-linked dimers as expected. We analysed their structure using CD spectroscopy, and, although there are some differences, the predicted secondary structure content is relatively similar for all mutants (Supplementary Figure S7A). Mutant 3 (a double mutant in the type I receptor site) has the most differing CD spectrum, and predicted to have significantly reduced helical content. Since the two mutations in this mutant are interacting with each other, across the wrist epitope α-helix, the reduced helical content is not entirely surprising. As seen below, this mutant had a similar effect on binding as other type I mutants, and hence the differing secondary structure does not appear to correlate with reduced binding properties of the protein. To validate the mutants biologically, the activity of each of the BMP-2 mutants was analysed using the C2C12 cell differentiation assay. As expected from mutations affecting the receptor-binding site, all mutants were shown to be inactive or with greatly reduced activity compared with wild-type protein (Supplementary Figure S7B–S7C). Only mutant 2 (L66R) in the type I receptor-interaction site showed measurable activity, but even that was almost two orders of magnitude lower than that of the wild-type BMP-2.

We then used the same BLI binding assay to measure the affinity of each of the mutants for fl-Gremlin-1 and ΔN-Gremlin-1 (Table 3 and Supplementary Figure S8). These experiments show that Gremlin-1 can still interact with the BMP-2 mutants, albeit with lower binding affinities. BMP-2s with mutations in the type I receptor-binding site had approximately 15-fold lower binding affinities than wild-type BMP-2, whereas the type II receptor-binding site mutants exhibited 30–60-fold reduction in affinity. This suggests that the residues in both BMP-2 receptor-binding sites are involved in Gremlin-1 binding. Since Gremlin-1 and BMP-2 mutants still interact with one another, the idea that Gremlin-1 blocks only one of the receptor-binding sites was not conclusively proven; no single mutant was able to abolish the binding completely, raising the question as to whether there could be an alternative mechanism by which BMP-2 signalling is inhibited.

Biophysical analysis of the BMP-2–ΔN-Gremlin-1 complex

AUC was used to measure sedimentation velocity of ΔN-Gremlin-1, BMP-2 and complex samples in 50 mM acetate buffer, pH 5.0, as DLS data showed the complex to be mostly monodisperse under these buffer conditions. Both AUC and DLS measurements gave similar information about the behaviour of the protein. ΔN-Gremlin-1 has one sharp dimer peak with molecular mass of 37 kDa (calculated molecular mass is 35 kDa) with minor traces of monomeric and tetrameric species (Supplementary Figure S9). BMP-2 has a broader and much less distinctive peak corresponding to a higher oligomeric form with minor traces of smaller particles. The molecular mass estimated from these data is approximately 380.0 kDa. With an expected molecular mass of 26 kDa for a dimer, it appears that at pH 5.0 BMP-2 forms aggregates. Interestingly, the complex sample contains lower-molecular-mass particles than BMP-2 alone. The large broad peak has a maximum at 147 kDa and only minor traces of smaller species are visible (according to the molecular mass these may represent an excess of ΔN-Gremlin-1). The data suggest that Gremlin-1 and BMP-2 oligomerize, differently to the expected one BMP-2 dimer one Gremlin-1 dimer complex which would have a molecular mass of 62 kDa. The data are not definitive and does not represent the real stoichiometry, but show that Gremlin-1 at least partially reduces BMP-2 aggregation by sequestering it into a larger complex, possibly at a stoichiometry close to 2:2 (Gremlin-1 dimers/BMP-2 dimers).

The AUC data led to the hypothesis that Gremlin-1 and BMP-2 form large complexes. To study this further, we turned again to BLI analysis. Although in a typical BLI experiment one measures first the association rate of the analyte to the immobilized binding partner followed by measurement of the dissociation rate in solution without the analyte, we decided to measure multiple association phases by alternating BMP-2 and Gremlin-1 as analytes. First, His-tagged ΔN-Gremlin-

Table 3 Analysis of fl-Gremlin-1- and ΔN-Gremlin-1-binding BMP-2 and BMP-2 mutants

	K_{on} (1/[M×s])		K_{off} (1/s)		K_d (nM)*		K_d (nM)†	
BMP-2	fl-Gremlin-1	ΔN-Gremlin-1	fl-Gremlin-1	ΔN-Gremlin-1	fl-Gremlin-1	ΔN-Gremlin-1	fl-Gremlin-1	ΔN-Gremlin-1
Wild-type	2.0×10^5	3.0×10^5	1.8×10^{-3}	5.0×10^{-3}	9.0	16.7	5.6	5.2
Mutant # 1	2.0×10^4	9.0×10^3	1.7×10^{-3}	7.0×10^{-4}	85.0	77.8	66.1	75.4
Mutant # 2	4.0×10^4	2.0×10^4	1.3×10^{-3}	6.0×10^{-4}	32.5	30.0	45.9	44.7
Mutant # 3	3.0×10^4	8.0×10^3	1.2×10^{-3}	1.4×10^{-3}	40.0	175	30.4	95.9
Mutant # 4	2.0×10^4	1.0×10^4	1.5×10^{-3}	2.3×10^{-3}	75.0	230	47.2	176
Mutant # 5	6.0×10^3	5.0×10^3	1.1×10^{-3}	1.0×10^{-3}	176	200	176	150
Mutant # 6	2.0×10^3	3.0×10^3	7.0×10^{-4}	8.0×10^{-4}	187	267	187	301
Mutant # 7	2.0×10^3	7.0×10^2	3.0×10^{-4}	2.0×10^{-4}	301	286	301	360

* K_d value calculated from the kinetics experiment. † K_d value estimated from the steady-state equilibrium equation.

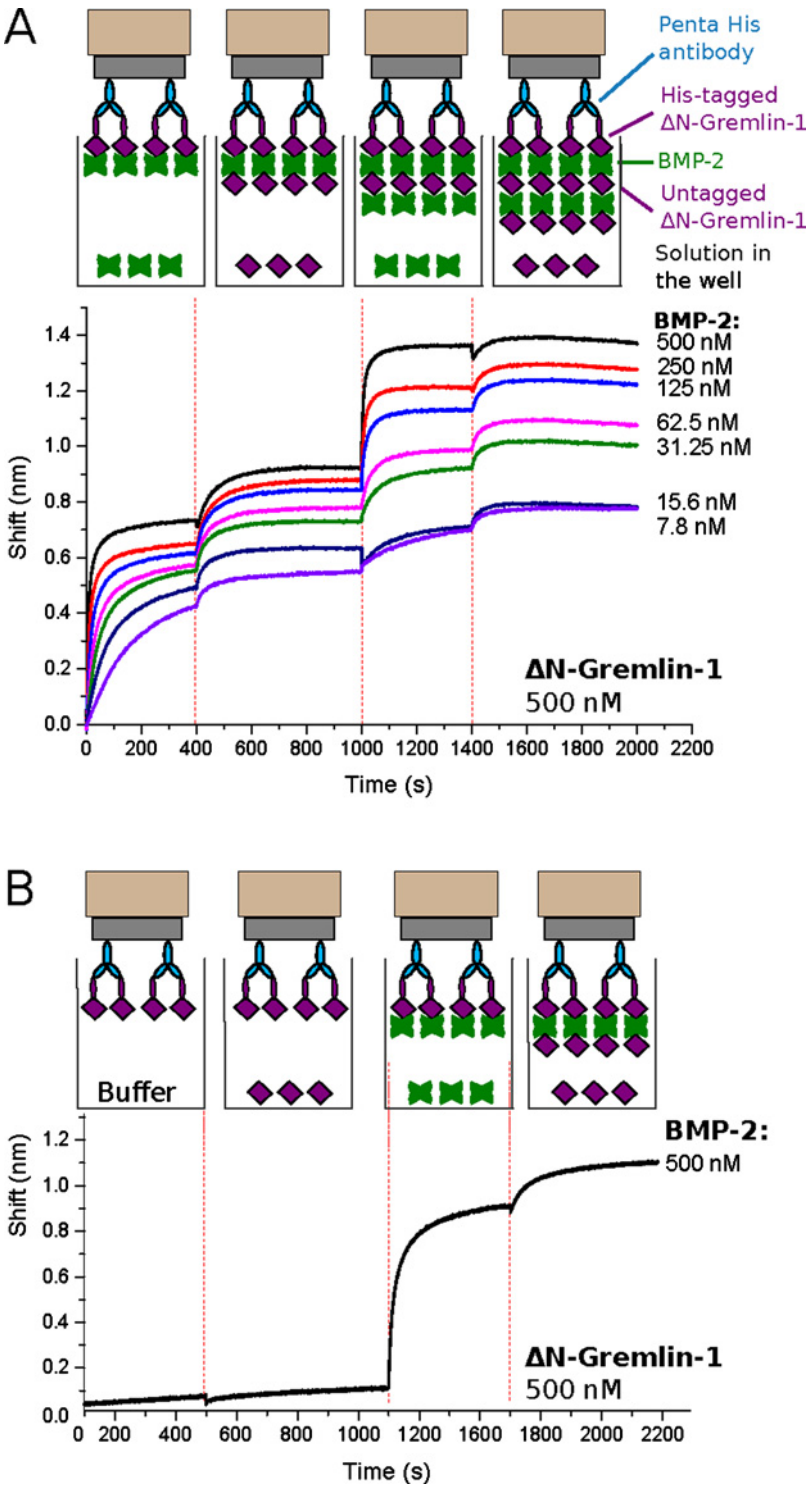

Figure 4 BLI analysis of repetitive ΔN-Gremlin-1 interaction with BMP-2

(**A**) Overview of the design of the repetitive binding experiment, with all of the components shown schematically. The curves show BLI response for each of the eight channels which differed in the concentration of BMP-2 in the well, as labelled at the end point of each curve. (**B**) Control experiment to determine non-specific ΔN-Gremlin-1 binding to His-tagged ΔN-Gremlin-1 or the tip surface.

1 was immobilized on biosensors using an anti-pentahistidine antibody. These sensors were then placed in wells containing different concentration of BMP-2 and association between the two proteins was recorded (as in previous experiments). Next, instead of measuring dissociation of the complex, the biosensors were moved directly into wells containing untagged ΔN-Gremlin-1 and association of Gremlin-1 with the sensors was monitored again. This sequence of incubating biosensor first in BMP-2 and then in untagged ΔN-Gremlin-1 was repeated once more (experimental set-up is depicted in Figure 4A). BMP-2 was used

at different concentrations (8–500 nM), whereas the concentration of Gremlin-1 was kept constant at 500 nM to ensure saturation of binding in this step, allowing allowed us to fit the binding of the second BMP-2 molecule with a steady-state model. Consecutive incubations of the biosensor in BMP-2 and in untagged ΔN-Gremlin-1 resulted in a continuous increase in the layer thickness on the biosensor tip, suggesting that untagged ΔN-Gremlin-1 bound to BMP-2 in an alternating manner. Steady-state model fitting showed that the first and second BMP-2 binding events had very similar affinities with K_d values of 5.2 nM and 8.5 nM respectively. Appropriate control experiments without untagged Gremlin-1 in between BMP-2 associations were also performed to ensure that the repeated binding is not due to non-specific interaction with the tips or BMP-2 or Gremlin-1 self-association (Figure 4B).

Results of the additive BLI experiment indicate that Gremlin-1 can bind to more than one BMP-2 molecule at the same time and vice versa. The K_d values of the first and the second binding of BMP-2 are in close agreement, suggesting that these are similar molecular events and support the hypothesis that Gremlin-1 and BMP-2 form an oligomeric complex. The same repetitive binding analysis was performed with all BMP-2 mutants and showed the same increase in layer thickness with each binding step (results not shown). Furthermore, K_d values of the second binding of BMP-2 mutants were in close agreement with the binding affinities measured in the first His-tagged Gremlin-1 and BMP-2 interaction, demonstrating that mutations in the receptor-binding sites of BMP-2 do not affect Gremlin-1 and BMP-2 oligomerization.

DISCUSSION

During the course of the present study, binding and inhibition assays were performed with two Gremlin-1 constructs to assess the role of the unique N-terminal segment in BMP-2 binding. The N-terminal sequence of 47 amino acids had no noticeable effect on the binary Gremlin-1 and BMP-2 interaction, indicating that the N-terminus of Gremlin-1 does not directly participate in the interaction. This is in clear contrast with the well-characterized cysteine knot inhibitor Noggin, which interacts with BMP-2 using flexible N-terminal segments to cover both the type I and type II receptor-binding sites [29]. In our cellular assay, however, fl-Gremlin-1 was approximately twice as active as ΔN-Gremlin-1, indicating that the N-termini of Gremlin-1 dimer may be involved in mediating other interactions with the extracellular environment (e.g. heparan sulfate binding), possibly co-localizing BMP-2 and Gremlin-1 and thus increasing the likelihood of inhibition within a biological context.

Several groups have shown that Gremlin-1 binds to heparin with 20 nM binding affinity, proving that such Gremlin-1 interaction with the extracellular environment is important for localization of BMP activity gradients in tissue [42]. Tatsinkam et al. [46] proposed that the heparin-binding site was located in three clusters of positively charges residues, mapping these on to our Gremlin-1 structure. The first cluster is in the C-terminus of the N-terminal α-helix and the two other clusters are mapped on to the second finger [45,46,48]. The same position for heparin-binding site has also been reported for another DAN family antagonist Sclerostin [24]. Unfortunately, it has not been investigated whether the N-terminus in particular has any effect on the Gremlin-1 (or other related antagonists) interaction with heparin. Given that the N-terminus is close to the proposed heparin-binding sites in Gremlin-1, it is possible that it does contribute to heparin binding and affect the behaviour of this protein in the tissue. Given that this is the most divergent part between DAN family members, a more detailed analysis of its role might reveal functional differences between these proteins.

Biophysical analyses showed that Gremlin-1 forms a stable non-covalent dimer in solution and structure determination of the conserved cystine knot part of the protein revealed an arch-shaped structure, composed mainly of β-sheets. The structure is very similar to that of Gremlin-2, as was predicted based on the high sequence similarity between these proteins. Although structures of many Dan family proteins have been determined, it remains unclear as to how they block BMP-2 signalling. The structure of Gremlin-1 in complex with BMP-2 would provide considerably more insight into the binding mechanism. Unfortunately, crystallization trials of the BMP-2–Gremlin-1 complex were not successful. One likely reason for the failure to crystallize the complex lies in the heterogeneity of the sample, as illustrated by the complex AUC data; it was not possible to co-purify the complex. These limitations in structural analysis encouraged us to analyse the complex using mutagenesis of BMP-2 and by different biophysical analysis.

Novel BMP-2 mutants that had either type I or type II receptor-binding site residues mutated were generated and shown to be inactive or have significantly reduced activity in the mouse myoblast bioassay. When these mutants were tested for their ability to interact with Gremlin-1, the binding was only partially disrupted by receptor site mutations, with reduced binding affinities, but none of the mutations resulted in total loss of binding. This suggests that there might be an alternative mechanism of BMP-2 inhibition to directly occluding the receptor interaction sites. Mutagenesis of Gremlin-2 (PRDC) has been similarly inconclusive, with no clear hot-spot being identified so far [31].

A significant number of studies have been performed to increase our understanding of the BMP signalling pathway and the role of extracellular antagonists in modulation of signalling. Previous findings show that many antagonists function through direct inhibition of BMPs by blocking their receptor-binding sites. Noggin undergoes ‘head-to-head’ dimerization which results in an arch-shaped dimer that shields the concave face of the active BMP-7 dimer. Furthermore, Noggin has flexible N-terminal ‘clip’ segments that form hydrophobic interactions with the BMPR-I (BMP receptor I)-binding pocket [20]. These N-termini wrap around the BMP-7 dimer and are suggested to be responsible for the high-affinity interaction. CV-2 binds to BMP-2 using its von Willebrand factor type C domain (VWC-1), with flexible N-terminal ‘clips’ of the VWC-1 wrapping around BMP, blocking both type I and II receptor-binding sites [33]. Follistatin antagonizes many TGF-β ligands, including activins, Myostatin and BMPs, using a distinctly different mode of interaction with its ligands to achieve inhibition. All four globular domains of follistatin participate in ligand binding with flexible linkers allowing a pair of follistatin molecules to wrap around the mature growth factor, blocking both type I and II receptor-binding pockets [49,50].

None of the aforementioned inhibition mechanisms seem to be applicable to the Gremlin-1 and BMP-2 interaction. The shape of Gremlin-1 is not unlike the shape of its ligand, BMP-2, and it is difficult to imagine geometrically how two such curved and elongated structures, both with internal two-fold symmetry could bind the other dimer with 1:1 stoichiometry while occluding receptor-binding sites which lie in the opposite sides of the BMP-2 dimer. Binding experiments show that both short and full-length Gremlin-1 constructs exhibit near identical binary interactions with BMP-2 and that the flexible N-terminal sequence does not influence ligand binding as is the case for

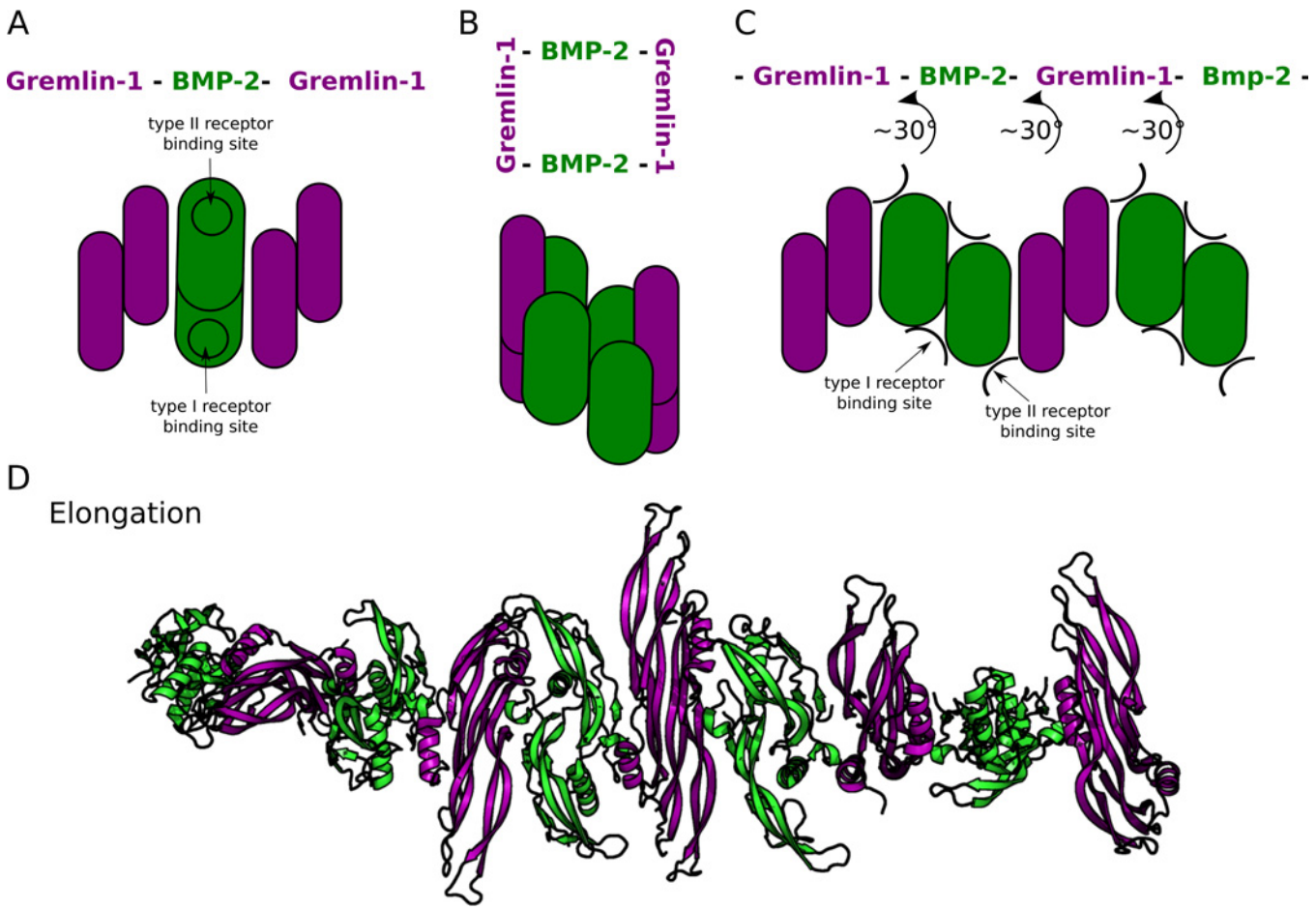

Figure 5 Model of ΔN-Gremlin-1 and BMP-2 oligomeric complex

(**A**) Complex model of 2:1 stoichiometry (two Gremlin-1 dimers: one BMP-2 dimer). (**B**) Complex model of 2:2 stoichiometry. (**C**) Model of complex oligomerization in 'fibril-like' manner. (**D**) Elongated model of 'fibril-like' complex formation based on crystal structure analysis. All models created 'manually' by orienting molecules to approximate locations and hence used for illustrative purposes only and not to be seen as precise atomic models.

Noggin or CV-2. Additionally, the arched Gremlin-1 dimer is more rigid than a multi-domain follistatin, and thus unlikely to change its conformation significantly upon binding to the ligand. AUC experiments showed that Gremlin-1 and BMP-2 form large complexes in solution raising the idea of Gremlin-1 sequestering BMP-2 into an oligomeric complex and thus preventing receptor interaction and signalling. Cell surface clustering of BMP-2 by repulsive guidance molecule (RGM) and neogenin has been suggested recently [51]. Such a clustering model seemed plausible for the complex of Gremlin-1 and BMP-2 as well and was tested using specially designed biosensor experiments. The results of additive BLI experiments showed incremental layer formation, indicating that Gremlin-1 can bind to more than one BMP-2 molecule at a time and vice versa, resulting in an alternating oligomer of Gremlin-1 and BMP-2. The affinities of the first and the second BMP-2 binding events were similar, suggesting that, at the molecular level, these events are equivalent. Higher oligomeric complexes of Gremlin-1 and BMP-2 might function differently depending on the concentration of Gremlin-1 and thus exert more complex regulation on the growth factor, beyond simply inhibiting its activity. Agonists of BMPs can facilitate endocytic uptake of the growth factors in a dose-dependent manner, but with Gremlin this process seems to be inhibited at higher concentrations [18]. No explanation for this has been revealed, but it is intriguing to think that our model of oligomerization could provide a clue to this differing behaviour, in comparison with other types of BMP inhibitors.

Taking these results together, we can envisage several possible models of Gremlin-1 and BMP-2 association, depicted in Figure 5. A closed 2:2 oligomeric complex of BMP-2–Gremlin-1 dimers is one possibility, in accordance with the size of the complex seen in AUC experiments, but a 'fibril-like' open-ended oligomer is an equally plausible model based on the BLI data (Figures 5C and 5D).

It is easy to imagine the 'fibril-like' architecture of the BMP-2–Gremlin-1 complex due to the arrangement of α-helices in these proteins. The α-helix in BMP-2 is important for interaction with receptors, given that it forms the binding pocket and interacts with the α-helix of BMPR-I [5]. Previous structural studies of BMP signalling modulators have shown that α-helix binding in the type I receptor pocket of the BMP dimer plays an important role in inhibition. The N-terminal α-helix which is present in both Gremlin-1 and Gremlin-2 is suggested to be flexible and poorly defined in the structure of Gremlin-2 [31]. The α-helix of Gremlin-1 could be placed in the BMPR-I-binding pocket, causing side-to-side binding of BMP-2 and Gremlin-1 (Figure 5D). The convex face of Gremlin-1 would then shield the hydrophobic patches of the knuckle epitope of BMP-2. Interaction of the α-helix probably

has an additional effect on Gremlin-1 and BMP-2 binding affinity, based on the findings of previous studies. First, Dan protein was shown to be less potent than Gremlin-2 [30]. The structure of Dan is very similar to the Gremlins (Figure 2), but Dan lacks the aforementioned α-helix. The same applies to another Dan family antagonist, Sclerostin, which also lacks the α-helix. This could be the reason Dan and Sclerostin are weaker antagonists, although both Gremlins form very-high-affinity interactions with BMPs. Mutations in Gremlin-2 and Dan also show that residues on the convex faces of these proteins are important for BMP-2 binding, supporting the proposed model of complex formation, but further studies are needed to evaluate these experimentally. Electron microscopy could be used to evaluate whether the complex forms such 'fibril-like' structures and further crystallographic studies are also required to elucidate the atomic details of the BMP-2 and Dan family proteins binding mechanism.

AUTHOR CONTRIBUTION

Miglė Kišonaitė did all the experiments under the supervision of Marko Hyvönen. Xuelu Wang performed CD experiments of BMP-2 mutants. Miglė Kišonaitė and Marko Hyvönen designed the experiments and wrote the paper. All authors participated in discussions and refinement of the paper.

ACKNOWLEDGEMENTS

We thank members of the Hyvönen laboratory for the help and advice, in particular Ms Katharina Ravn for the original wild-type BMP-2 preparation and Dr Gerhard Fischer for his help with crystallography and SAXS data processing. We are grateful to Dr Katri Koli for providing us with the cDNA clone of Gremlin-1. We also acknowledge Dr Grahame McKenzie, MRC Cancer Unit, University of Cambridge, who provided the C2C12 mouse myoblast cells. We thank the Diamond Light Source and the beamline staff for access to beamline I04 (proposal mx9537) and beamline I22 for SAXS measurements.

FUNDING

This work was supported by the Cambridge European Trust through a postgraduate scholarship (to M.K.); and the China Scholarship Council scholarship (to X.W.).

REFERENCES

1 Dionne, M.S., Skarnes, W.C. and Harland, R.M. (2001) Mutation and analysis of Dan, the founding member of the Dan family of transforming growth factor beta antagonists. Mol. Cell. Biol. **21**, 636–643 CrossRef PubMed
2 Nolan, K. and Thompson, T.B. (2014) The DAN family: modulators of TGF-β signaling and beyond. Protein Sci. **23**, 999–1012 CrossRef PubMed
3 Rider, C.C. and Mulloy, B. (2010) Bone morphogenetic protein and growth differentiation factor cytokine families and their protein antagonists. Biochem. J. **429**, 1–12 CrossRef PubMed
4 Walsh, D.W., Godson, C., Brazil, D.P. and Martin, F. (2010) Extracellular BMP-antagonist regulation in development and disease: tied up in knots. Trends Cell Biol. **20**, 244–256 CrossRef PubMed
5 Allendorph, G.P., Vale, W.W. and Choe, S. (2006) Structure of the ternary signaling complex of a TGF-β superfamily member. Proc. Natl. Acad. Sci. U.S.A. **103**, 7643–7648 CrossRef PubMed
6 Bragdon, B., Moseychuk, O., Saldanha, S., King, D., Julian, J. and Nohe, A. (2011) Bone morphogenetic proteins: a critical review. Cell. Signal. **23**, 609–620 CrossRef PubMed
7 Chen, H., Brady Ridgway, J., Sai, T., Lai, J., Warming, S., Chen, H., Roose-Girma, M., Zhang, G., Shou, W. and Yan, M. (2013) Context-dependent signaling defines roles of BMP9 and BMP10 in embryonic and postnatal development. Proc. Natl. Acad. Sci. U.S.A. **110**, 11887–11892 CrossRef PubMed
8 Derynck, R. and Feng, X.H. (1997) TGF-beta receptor signaling. Biochim. Biophys. Acta **1333**, F105–F150 PubMed
9 Harrison, C.A., Wiater, E., Gray, P.C., Greenwald, J., Choe, S. and Vale, W. (2004) Modulation of activin and BMP signaling. Mol. Cell. Endocrinol. **225**, 19–24 CrossRef PubMed
10 Hogan, B.L. (1996) Bone morphogenetic proteins in development. Curr. Opin. Genet. Dev. **6**, 432–438 CrossRef PubMed
11 Macias, M.J., Martin-Malpartida, P. and Massagué, J. (2015) Structural determinants of Smad function in TGF-β signaling. Trends Biochem. Sci. **40**, 296–308 CrossRef PubMed
12 Cai, J., Pardali, E., Sánchez-Duffhues, G. and ten Dijke, P. (2012) BMP signaling in vascular diseases. FEBS Lett. **586**, 1993–2002 CrossRef PubMed
13 Long, L., Ormiston, M.L., Yang, X., Southwood, M., Gräf, S., Machado, R.D., Mueller, M., Kinzel, B., Yung, L.M., Wilkinson, J.M. et al. (2015) Selective enhancement of endothelial BMPR-II with BMP9 reverses pulmonary arterial hypertension. Nat. Med. **21**, 777–785 CrossRef PubMed
14 Xiao, Y.-T., Xiang, L.-X. and Shao, J.-Z. (2007) Bone morphogenetic protein. Biochem. Biophys. Res. Commun. **362**, 550–553 CrossRef PubMed
15 Allendorph, G.P., Isaacs, M.J., Kawakami, Y., Izpisua Belmonte, J.C. and Choe, S. (2007) BMP-3 and BMP-6 structures illuminate the nature of binding specificity with receptors. Biochemistry **46**, 12238–12247 CrossRef PubMed
16 Nickel, J., Sebald, W., Groppe, J.C. and Mueller, T.D. (2009) Intricacies of BMP receptor assembly. Cytokine Growth Factor Rev. **20**, 367–377 CrossRef PubMed
17 Nohe, A., Hassel, S., Ehrlich, M., Neubauer, F., Sebald, W., Henis, Y.I. and Knaus, P. (2002) The mode of bone morphogenetic protein (BMP) receptor oligomerization determines different BMP-2 signaling pathways. J. Biol. Chem. **277**, 5330–5338 CrossRef PubMed
18 Alborzinia, H., Schmidt-Glenewinkel, H., Ilkavets, I., Breitkopf-Heinlein, K., Cheng, X., Hortschansky, P., Dooley, S. and Wölfl, S. (2013) Quantitative kinetics analysis of BMP2 uptake into cells and its modulation by BMP antagonists. J. Cell Sci. **126**, 117–127 CrossRef PubMed
19 Bier, E. (2008) Intriguing extracellular regulation of BMP signaling. Dev. Cell **15**, 176–177 CrossRef PubMed
20 Groppe, J., Greenwald, J., Wiater, E., Rodriguez-Leon, J., Economides, A.N., Kwiatkowski, W., Affolter, M., Vale, W.W., Izpisua Belmonte, J.C. and Choe, S. (2002) Structural basis of BMP signalling inhibition by the cystine knot protein Noggin. Nature **420**, 636–642 CrossRef PubMed
21 Yanagita, M. (2005) BMP antagonists: their roles in development and involvement in pathophysiology. Cytokine Growth Factor Rev. **16**, 309–317 CrossRef PubMed
22 Hsu, D.R., Economides, A.N., Wang, X., Eimon, P.M. and Harland, R.M. (1998) The Xenopus dorsalizing factor Gremlin identifies a novel family of secreted proteins that antagonize BMP activities. Mol. Cell **1**, 673–683 CrossRef PubMed
23 Müller, I., Schönberger, T., Schneider, M., Borst, O., Ziegler, M., Seizer, P., Leder, C., Müller, K., Lang, M., Appenzeller, F. et al. (2013) Gremlin-1 is an inhibitor of macrophage migration inhibitory factor and attenuates atherosclerotic plaque growth in ApoE-/- mice. J. Biol. Chem. **288**, 31635–31645 CrossRef PubMed
24 Wellbrock, J., Harbaum, L., Stamm, H., Hennigs, J.K., Schulz, B., Klose, H., Bokemeyer, C., Fiedler, W. and Lüneburg, N. (2015) Intrinsic BMP antagonist gremlin-1 as a novel circulating marker in pulmonary arterial hypertension. Lung **193**, 567–570 CrossRef PubMed
25 Kosinski, C., Li, V.S., Chan, A.S., Zhang, J., Ho, C., Tsui, W.Y., Chan, T.L., Mifflin, R.C., Powell, D.W., Yuen, S.T. et al. (2007) Gene expression patterns of human colon tops and basal crypts and BMP antagonists as intestinal stem cell niche factors. Proc. Natl. Acad. Sci. U.S.A. **104**, 15418–15423 CrossRef PubMed
26 Davis, H., Irshad, S., Bansal, M., Rafferty, H., Boitsova, T., Bardella, C., Jaeger, E., Lewis, A., Freeman-Mills, L., Giner, F.C. et al. (2015) Aberrant epithelial GREM1 expression initiates colonic tumorigenesis from cells outside the stem cell niche. Nat. Med. **21**, 62–70 CrossRef PubMed
27 Sneddon, J.B., Zhen, H.H., Montgomery, K., Rijn, M., van de, Tward, A.D., West, R., Gladstone, H., Chang, H.Y., Morganroth, G.S., Oro, A.E. et al. (2006) Bone morphogenetic protein antagonist gremlin 1 is widely expressed by cancer-associated stromal cells and can promote tumor cell proliferation. Proc. Natl. Acad. Sci. U.S.A. **103**, 14842–14847 CrossRef PubMed
28 Veverka, V., Henry, A.J., Slocombe, P.M., Ventom, A., Mulloy, B., Muskett, F.W., Muzylak, M., Greenslade, K., Moore, A., Zhang, L. et al. (2009) Characterization of the structural features and interactions of sclerostin: molecular insight into a key regulator of Wnt-mediated bone formation. J. Biol. Chem. **284**, 10890–10900 CrossRef PubMed
29 Weidauer, S.E., Schmieder, P., Beerbaum, M., Schmitz, W., Oschkinat, H. and Mueller, T.D. (2009) NMR structure of the Wnt modulator protein Sclerostin. Biochem. Biophys. Res. Commun. **380**, 160–165 CrossRef PubMed
30 Nolan, K., Kattamuri, C., Luedeke, D.M., Angerman, E.B., Rankin, S.A., Stevens, M.L., Zorn, A.M. and Thompson, T.B. (2015) Structure of neuroblastoma suppressor of tumorigenicity 1 (NBL1): insights for the functional variability across bone morphogenetic protein (BMP) antagonists. J. Biol. Chem. **290**, 4759–4771 CrossRef PubMed
31 Nolan, K., Kattamuri, C., Luedeke, D.M., Deng, X., Jagpal, A., Zhang, F., Linhardt, R.J., Kenny, A.P., Zorn, A.M. and Thompson, T.B. (2013) Structure of protein related to Dan and Cerberus: insights into the mechanism of bone morphogenetic protein antagonism. Structure **21**, 1417–1429 CrossRef PubMed

32 Sharma, A., Meyer, F., Hyvonen, M., Best, S.M., Cameron, R.E. and Rushton, N. (2012) Osteoinduction by combining bone morphogenetic protein (BMP)-2 with a bioactive novel nanocomposite. Bone Joint Res. **1**, 145–151 CrossRef PubMed

33 Zhang, J.-L., Qiu, L.-Y., Kotzsch, A., Weidauer, S., Patterson, L., Hammerschmidt, M., Sebald, W. and Mueller, T.D. (2008) Crystal structure analysis reveals how the Chordin family member crossveinless 2 blocks BMP-2 receptor binding. Dev. Cell **14**, 739–750 CrossRef PubMed

34 Peränen, J., Rikkonen, M., Hyvönen, M. and Kääriäinen, L. (1996) T7 vectors with modified T7*lac* promoter for expression of proteins in Escherichia coli. Anal. Biochem. **236**, 371–373 CrossRef PubMed

35 Brinkmann, U., Mattes, R.E. and Buckel, P. (1989) High-level expression of recombinant genes in Escherichia coli is dependent on the availability of the dnaY gene product. Gene **85**, 109–114 CrossRef PubMed

36 Katagiri, T., Yamaguchi, A., Komaki, M., Abe, E., Takahashi, N., Ikeda, T., Rosen, V., Wozney, J.M., Fujisawa-Sehara, A. and Suda, T. (1994) Bone morphogenetic protein-2 converts the differentiation pathway of C2C12 myoblasts into the osteoblast lineage. J. Cell. Biol. **127**, 1755–1766 CrossRef PubMed

37 Vonrhein, C., Flensburg, C., Keller, P., Sharff, A., Smart, O., Paciorek, W., Womack, T. and Bricogne, G. (2011) Data processing and analysis with the autoPROC toolbox. Acta Crystallogr. D Biol. Crystallogr. **67**, 293–302 CrossRef PubMed

38 Murshudov, G.N., Skubák, P., Lebedev, A.A., Pannu, N.S., Steiner, R.A., Nicholls, R.A., Winn, M.D., Long, F. and Vagin, A.A. (2011) REFMAC5 for the refinement of macromolecular crystal structures. Acta Crystallogr. D Biol. Crystallogr. **67**, 355–367 CrossRef PubMed

39 Emsley, P. and Cowtan, K. (2004) Coot: model-building tools for molecular graphics. Acta Crystallogr. D Biol. Crystallogr. **60**, 2126–2132 CrossRef PubMed

40 Petoukhov, M.V., Franke, D., Shkumatov, A.V., Tria, G., Kikhney, A.G., Gajda, M., Gorba, C., Mertens, H.D.T., Konarev, P.V. and Svergun, D.I. (2012) New developments in the ATSAS program package for small-angle scattering data analysis. J. Appl. Crystallogr. **45**, 342–350 CrossRef PubMed

41 Schuck, P. (2004) A model for sedimentation in inhomogeneous media. I. Dynamic density gradients from sedimenting co-solutes. Biophys. Chem. **108**, 187–200 CrossRef PubMed

42 Church, R.H., Krishnakumar, A., Urbanek, A., Geschwindner, S., Meneely, J., Bianchi, A., Basta, B., Monaghan, S., Elliott, C., Stromstedt, M. et al. (2015) Gremlin1 preferentially binds to bone morphogenetic protein-2 (BMP-2) and BMP-4 over BMP-7. Biochem. J. **466**, 55–68 CrossRef PubMed

43 Binnerts, M.E., Wen, X., Canté-Barrett, K., Bright, J., Chen, H.-T., Asundi, V., Sattari, P., Tang, T., Boyle, B., Funk, W. et al. (2004) Human Crossveinless-2 is a novel inhibitor of bone morphogenetic proteins. Biochem. Biophys. Res. Commun. **315**, 272–280 CrossRef PubMed

44 Nakamura, K., Shirai, T., Morishita, S., Uchida, S., Saeki-Miura, K. and Makishima, F. (1999) p38 mitogen-activated protein kinase functionally contributes to chondrogenesis induced by growth/differentiation factor-5 in ATDC5 cells. Exp. Cell Res. **250**, 351–363 CrossRef PubMed

45 Chiodelli, P., Mitola, S., Ravelli, C., Oreste, P., Rusnati, M. and Presta, M. (2011) Heparan sulfate proteoglycans mediate the angiogenic activity of the vascular endothelial growth factor receptor-2 agonist gremlin. Arterioscler. Thromb. Vasc. Biol. **31**, e116–e127 CrossRef PubMed

46 Tatsinkam, A.J., Mulloy, B. and Rider, C.C. (2015) Mapping the heparin-binding site of the BMP antagonist gremlin by site-directed mutagenesis based on predictive modelling. Biochem. J. **470**, 53–64 CrossRef PubMed

47 Laskowski, R.A. and Swindells, M.B. (2011) LigPlot + : multiple ligand-protein interaction diagrams for drug discovery. J. Chem. Inf. Model. **51**, 2778–2786 CrossRef PubMed

48 Ruppert, R., Hoffmann, E. and Sebald, W. (1996) Human bone morphogenetic protein 2 contains a heparin-binding site which modifies its biological activity. Eur. J. Biochem. **237**, 295–302 CrossRef PubMed

49 Harrington, A.E., Morris-Triggs, S.A., Ruotolo, B.T., Robinson, C.V., Ohnuma, S.-I. and Hyvönen, M. (2006) Structural basis for the inhibition of activin signalling by follistatin. EMBO J. **25**, 1035–1045 CrossRef PubMed

50 Lerch, T.F., Shimasaki, S., Woodruff, T.K. and Jardetzky, T.S. (2007) Structural and biophysical coupling of heparin and activin binding to follistatin isoform functions. J. Biol. Chem. **282**, 15930–15939 CrossRef PubMed

51 Healey, E.G., Bishop, B., Elegheert, J., Bell, C.H., Padilla-Parra, S. and Siebold, C. (2015) Repulsive guidance molecule is a structural bridge between neogenin and bone morphogenetic protein. Nat. Struct. Mol. Biol. **22**, 458–465 CrossRef PubMed

Received 8 December 2015/28 March 2016; accepted 1 April 2016
Accepted Manuscript online 1 April 2016, doi:10.1042/BCJ20160254